2022

Design of an accelerator-based shielding experiment at the NASA Space Radiation Laboratory relevant to enclosed, shielded environments in space

Lawrence H Heilbronn
lheilbro@utk.edu

Michael Sivertz
Brookhaven National Laboratory

Adam Rusek
Brookhaven National Laboratory

Charlie Pearson
Brookhaven National Laboratory

Martha Clowdsley
NASA Langley Research Center

Design of an accelerator-based shielding experiment at the NASA Space Radiation Laboratory relevant to enclosed, shielded environments in space

Lawrence H. Heilbronn[1], Michael Sivertz[2], Adam Rusek[2], Charlie Pearson[2], Martha Clowdsley[3], Luis Castellanos[1], Natalie McGirl[1], Ashwin Srikrishna[1], Cary Zeitlin[4],

Affiliations:

1. University of Tennessee, 305 Nuclear Engineering Building, Knoxville, TN 37916
2. NASA Space Radiation Laboratory, Brookhaven National Laboratory, Upton, NY
3. NASA Langley Research Center, Hampton, VA
4. Leidos Innovations Corporation, Houston, TX

Corresponding author:

Lawrence H Heilbronn

Email: lheilbro@utk.edu

Address: 305 Nuclear Engineering Building, University of Tennessee, Knoxville, TN 37916, USA

Phone number: +01-865-974-0982

Abstract

Recent calculations indicate that the dose equivalent in an enclosed, shielded environment in a galactic cosmic ray field will increase or remain unchanged when shielding thickness increases beyond 20 to 30 g/cm^2. This trend is seen out to 100 g/cm^2, beyond which calculations were not run since depths greater than this are not envisioned for human missions in deep space. If these calculations are accurate, then an optimal shielding thickness (or narrow range of thicknesses) exists, with important implications for spacecraft and habitat design. Crucially, the calculation reveals a minimum dose equivalent value that cannot be reduced with added shielding, leaving mission duration as the only means of controlling accumulated dose equivalent so as to remain within recommended limits. In order to provide a benchmark set of experimental data that can be used to quantify the uncertainties in the calculations and provide some level of verification of their predictions, we have designed a series of experiments at the NASA Space Radiation Laboratory at Brookhaven National Laboratory to measure the light ion production created by GCR-like beams incident on a two-target system that mimics an enclosed, shielded environment. This paper gives detailed descriptions of the experimental configurations to provide accurate input data for transport models. Subsequent articles report the measurement results and comparisons to models.

I Introduction

Slaba et al. [1] performed calculations with several transport models that predict the dose equivalent created by galactic cosmic rays (GCR) incident upon either a spherical shell of varying shielding thickness or upon two infinite slabs with a dose point located between the slabs. The thickness of the shielding ranged between 0 and 100 g/cm^2 in both the spherical and slab geometries. Figure 1 is a reproduction from Ref. [1] that illustrates the minimum in dose equivalent at approximately 20 g/cm^2 of aluminum shielding and the constant dose equivalent beyond 20 – 40 g/cm^2 of polyethylene shielding as predicted by several transport model calculations, including FLUKA [2], Geant4 [3], MCNP6 [4], PHITS [5], and 3DHZETRN [6].

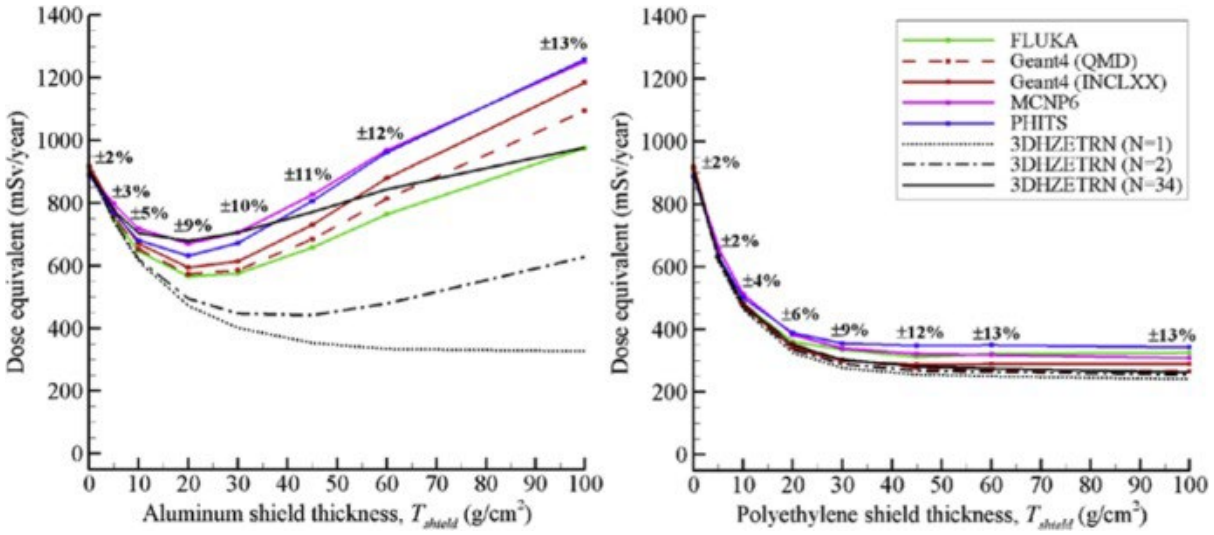

Figure 1. Dose equivalent from neutrons and ions as a function of aluminum (left) and polyethylene (right) shield thickness for the full GCR boundary condition.

All model calculations display the same trends, but differences exist between the codes in the predicted magnitudes of the dose equivalent, particularly in the region beyond the minimum when aluminum shielding is considered. A detailed analysis by Slaba indicated that the behavior of the dose equivalent beyond 20 g/cm^2 was due primarily to the production of neutrons and charged, light-ion secondary protons, deuterons, tritons, ^{3}He and ^{4}He. However, comparisons between calculations of inclusive light ion production from GCR-like interactions and either measured cross section data or data generated through benchmark thick-target experiments has not been explored to the level of detail as with measurements of heavier secondary particles [7]. Consequently, the source of greatest uncertainty with the transport

calculations shown in Ref. [1] is in the production of protons (p), deuterons (d), tritons (t), ^{3}He, ^{4}He and neutrons from proton and heavy ion interactions in shielding materials. To determine the uncertainty in GCR transport model calculations due to light ion production, as well as provide a set of benchmark data for comparisons to those models, we designed an accelerator-based experiment based on the concept of the radiation field created in an enclosed, shielded environment. The details of the design and execution of the experiments are described herein.

II Experimental Design

II.1 Measurement Objectives

The particle species and energies of interest in the measurement campaign were determined by both scientific needs and the capabilities of the instrumentation. Charged secondary light ions (p, d, t, He isotopes) and secondary neutrons were identified as the species of interest due to their significance in the results presented by [1], and because of the lack of secondary light ion data for comparison to GCR transport calculations [7,8]. Because of the wide range of beam particle species and energies and target thicknesses to be considered along with the limitations of available beamtime, both neutrons and charged secondaries were measured simultaneously. This requirement led to the choice of using a variety of scintillators and techniques capable of discriminating neutrons, gamma rays, and charged particles from each other. To optimize the discrimination capabilities of the system as well as to optimize the energy resolution of the measurements, energies of the particles were determined using time-of-flight and pulse height deconvolution techniques.

In total, secondary light ion production yields were measured from 120 systems, where a system is defined as a single combination of beam species, beam energy, upstream target material and target thickness.

II.2 Beams and Targets

The experiments used a two-target configuration to mimic the enclosed shielded environment simulated in the transport model calculations. The upstream and downstream targets were placed directly along the centerline of the beam, with the distance between the center of the upstream target and front face of the downstream target equal to 3.5 meters. Two target materials were chosen for the measurements. Aluminum was used as one of the target materials because of its common use in spacecraft, and polyethylene was used to

represent the class of hydrogenous shielding materials known for their superior capabilities to reduce the dose and dose equivalent from GCR [9,10]. Three thicknesses were used for pure Al and polyethylene upstream targets (20, 40 and 60 g/cm^2), and two thicknesses were used for combined Al+polyethylene upstream targets (20 and 60 g/cm^2). The combination target was chosen to simulate an environment with an aluminum shell surrounding materials inside a spacecraft, such as water and humans. One thickness (60 g/cm^2) was used for the downstream target, with an aluminum downstream target paired with upstream aluminum targets, and a polyethylene downstream target paired with upstream polyethylene and Al+polyethylene targets. Upstream target thicknesses were chosen to investigate the range of thicknesses that encompassed the predicted minimum in dose equivalent. Table 1 shows the target configurations used for each data set.

Table 1: The configurations of target materials and thicknesses used during the experiments conducted at the NSRL.

Upstream target material, thickness (g/cm^2)	Downstream target material, thickness (g/cm^2)
Al (20)	Al (60)
Al (40)	Al (60)
Al (60)	Al (60)
Polyethylene (20)	Polyethylene (60)
Polyethylene (40)	Polyethylene (60)
Polyethylene (60)	Polyethylene (60)
Al (10) + Polyethylene (10)	Polyethylene (60)
Al (10) + Polyethylene (50)	Polyethylene (60)

The beam species and energies were chosen to represent significant components of the GCR spectrum in terms of their contributions to the fluence as well as their significance in understanding the underlying physics used in transport model calculations. The beam species chosen were protons, ^{4}He, ^{12}C, ^{28}Si, and ^{56}Fe. The beam energies incident upon the beam exit window into the NSRL irradiation room are listed in Table 2.

Table 1. Beam species and energies used for the NSRL thick target measurements. Reported energies are the energies incident upon the beam line exit window into the NSRL irradiation room. Uncertainties for beam energies, indicated in parentheses, are less than or on the order of 1%

Beam species	Beam energies (MeV/nucleon)
Protons	400(3), 800(6), 2500(15)
^{4}He	400(3), 800(6), 1500(10)
^{12}C	400(3), 800(6), 1400(10)[a], 1500(10)
^{28}Si	400(3), 800(6), 1470(10)[b], 1500(10)
^{56}Fe	400(3), 800(6), 1470(10)[b], 1463(10)[c]

[a] energy used for pure polyethylene and (Al+polyethylene) combination upstream targets

[b] energy used for pure Al upstream targets

[c] energy used for pure polyethylene targets

II.3 Detectors

Figure 2 shows a schematic diagram of the placement of the detector systems in the NSRL irradiation room. Beam entered the room from the right at a height of 121.9 cm above the concrete floor, passing through a 381 μm-thick aluminum window at the end of the vacuum line and then traveling 383.8 cm to center between two thin, solid plastic scintillators labeled "Start scintillators" in the figure. The start scintillators (Eljen Technology EJ-228) were used for beam particle identification and in the time-of-flight analysis. Both scintillators were 0.2-cm thick. For C, Si and Fe beams, the start scintillators were placed 7.9-cm apart, with the upstream scintillator having areal dimensions of 4x4 cm^2 and the downstream detector having dimensions of 5x5 cm^2. For ^{1}H and ^{4}He beams, the start scintillators were placed 3-cm apart, with the upstream detector having areal dimensions of 1x1 cm^2 and the downstream detector having dimensions of 1.4x1.4 cm^2. For all systems, the distance from the midpoint between the start scintillators to the center of the upstream target was 78.45 cm for measurements made in March of 2016 and 76.2 cm for measurements made later in November-December 2016 and November 2017.

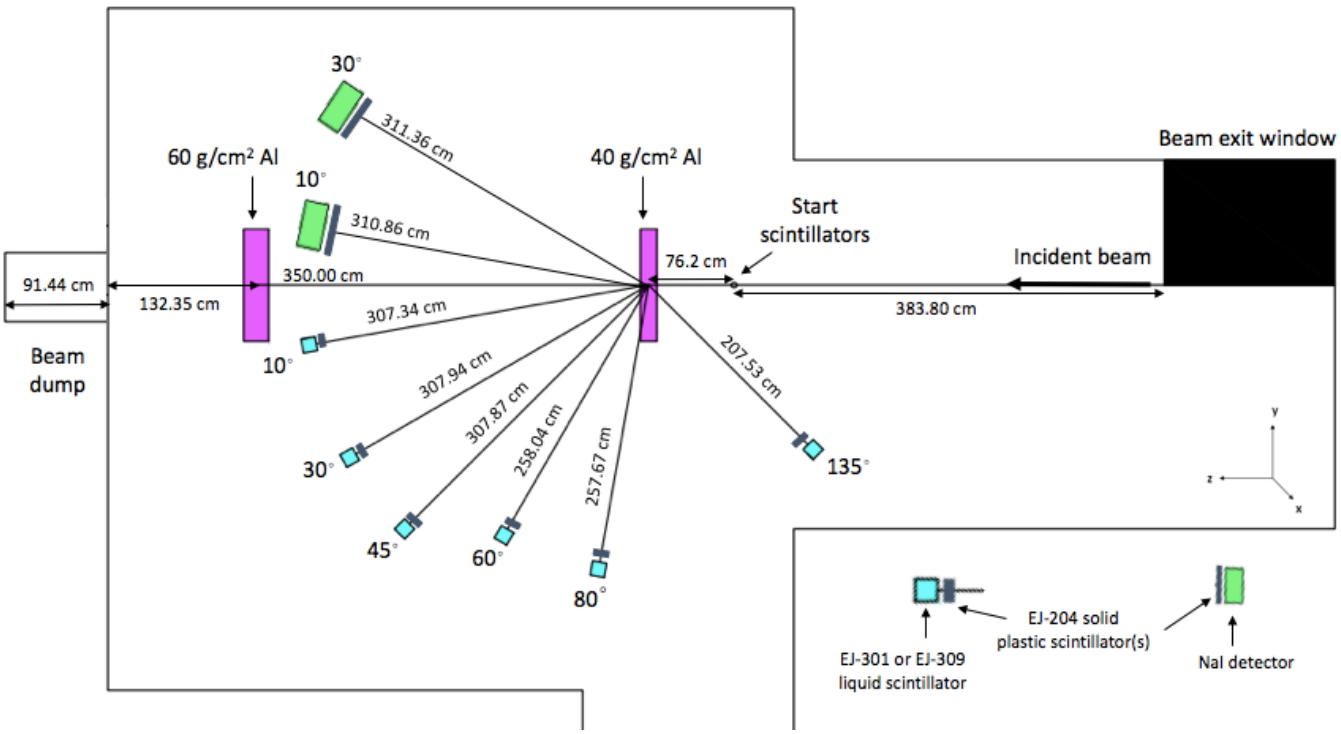

Figure 2. A schematic of the experimental setup in the NSRL irradiation room. Targets are shown in purple, liquid scintillators are shown in blue, and NaI detectors are shown in green. Solid plastic scintillators are shown in black. Not shown are the second solid plastic scintillators that were placed at the sides of the liquid scintillators

Six liquid scintillators (Eljen Technology EJ-309 and EJ-301) were used for neutron and charged particle detection. The EJ-301 scintillators were placed at 10°, 30°, and 45°, and the EJ-309 scintillators were placed at 60°, 80°, and 135° relative to the center of the upstream target and to the left of the beam, as shown in Figure 2. The centers of these detectors and all other detectors were placed in the plane of the beam, 121.9 cm above the concrete floor. The scintillators were right-circular cylinders with active volumes given by a width of 12.7 cm and a length of 12.7 cm. For each detector, the active volume of the cylinder was surrounded by an aluminum housing 0.152-cm thick. Technical information for the two types of liquid scintillators is given in Table 3.

Table 3. EJ-301 and EJ-309 liquid scintillator information

Detector type	Light output (% anthracene)	Density (g/cm^3)	C atoms per cm^3	H atoms per cm^3	# photons per 1 MeV electron
EJ-301	78	0.874	$3.98x10^{22}$	$4.82x10^{22}$	12,000
EJ-309	80	0.959	$4.35x10^{22}$	$5.43x10^{22}$	12,300
EJ-204	68	1.023	$4.68x10^{22}$	$5.15x10^{22}$	10,400

To discriminate between incident charged particles and neutrons, solid plastic scintillators were placed directly in front of the cylindrical face of the liquid scintillator, with the faces of both the liquid and solid scintillators (EJ-204) oriented on the line to the center of the upstream target. Technical information for the EJ-204 scintillators is given in Table 3. An identical solid plastic scintillator was placed at the side of the 30°, 45°, 60° and 80° liquid scintillators, facing the beam as the beam passed between the upstream and downstream targets. For the 10° detector, a second solid plastic scintillator was placed directly between the center of the downstream target and the center of the liquid scintillator. For the 135° detector, the second scintillator was placed at the side of the liquid scintillator facing the incoming beam. Distances between the liquid and solid scintillators were generally between 1 and 2 cm. Figure 3 shows a photograph of the 80°, 60° and 45° liquid-solid scintillator arrays along with the detector stands used to mount and align the detectors.

Figure 3. From left to right, the 80°, 60° and 45° liquid scintillator arrays with their accompanying solid plastic detectors. The liquid scintillators are the cylindrical detectors (aluminum housing), and the solid plastic scintillators are the black, 5-inch by 5-inch detectors

As shown in Fig. 2, two sodium iodide (NaI) detector arrays were placed to the right of the beam direction, with the centers of the arrays placed at 10° and 30°. As with the other detectors used in the measurements, the centers of the NaI arrays were placed at beam height. These detectors were used for secondary charged particle detection. Each NaI detector was a 10.16-cm x 10.16-cm x 40.64-cm rectangular block surrounded by a 0.159-cm thick aluminum housing. Each NaI array consisted of two NaI detectors placed side by side, with three solid plastic scintillators placed directly in front of the NaI detector closest to the upstream target. The faces of the plastic scintillators and NaI were oriented perpendicular to the line connecting their centers to the center of the upstream target. The data from the NaI served three purposes: (1) to extend the dynamic range of light charged-particle energies measured at 10° and 30°, (2) to provide finer granularity in the angular distributions of the spectra, and (3) to provide an internal consistency check of the methodologies used in the data analysis, by comparing with similar data from the liquid scintillators at 10° and 30°.

Figure 4 shows the 30° NaI array with the three solid plastic scintillators (black) aligned in front of the two NaI detectors (silver, with their PMTs and bases visible on the far right of the picture).

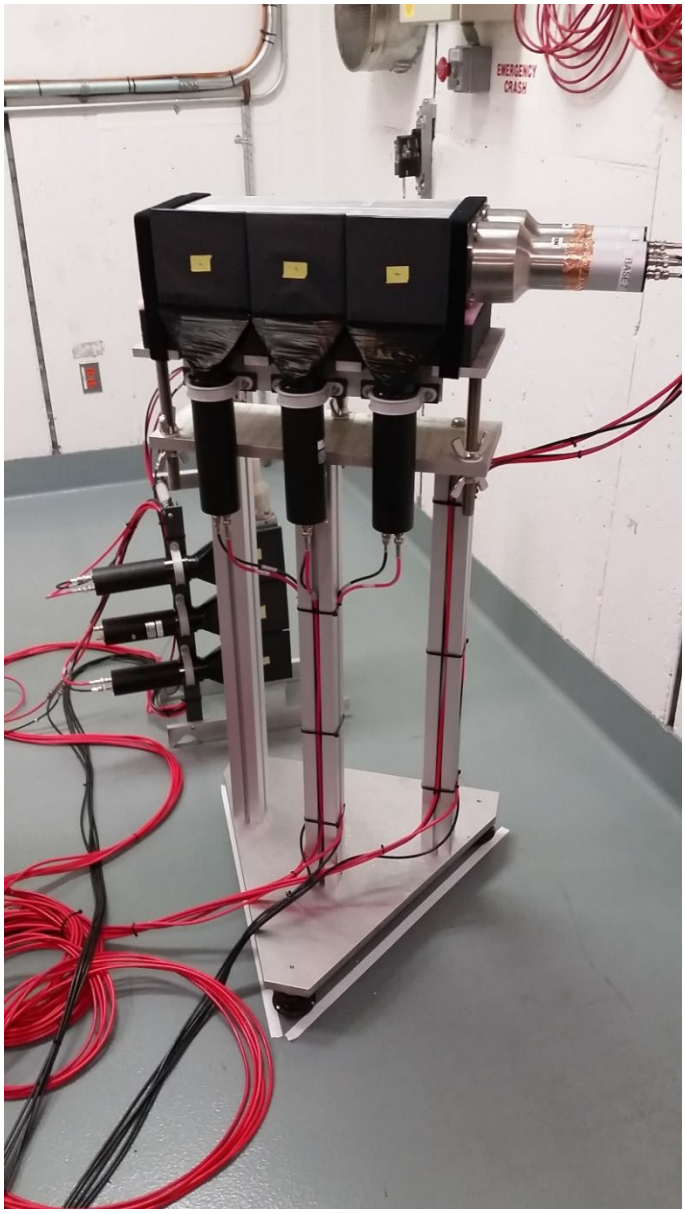

Figure 4. The 30° NaI detector array and stand. The three, square plastic scintillators are mounted directly in front of the two NaI detectors. The phototubes and bases for the NaI detectors can be seen at the right.

II.4 Room Dimensions

Because the measurements of neutrons unavoidably included the contribution from room-scattered neutrons, room dimensions are required inputs to the transport models used for

benchmark calculations. The main portion of the target room that contains the targets and detectors has a cross-sectional area of 6.1 x 6.1 m^2, with a floor-to-ceiling height of 3.05 m. A pair of 5.08-cm diameter steel rails are placed 0.87 m above the floor, running parallel along the beam axis from the beam exit location down to the front face of the downstream target. The rails are separated laterally by 40 cm and are used for mounting targets and other equipment directly along the beam axis. The entrance to the beam dump is 61x61 cm^2 (2x2 ft^2) and extends 91.4 cm (3 feet) into the concrete wall. Beyond the end of the beam dump there is 121.9 cm (4 feet) of concrete wall and concrete bricks, followed by 259.1 cm (4.5 feet) of iron. The concrete bricks and iron behind the beam dump are buried under soil. The concrete used for the walls, ceiling and floor has a density of 2.3, and the walls are 121.9 cm (4 feet) thick. The NSRL irradiation room is generally kept at a temperature between 68°F and 72°F, with an atmospheric pressure equal to ambient pressure at sea level.

II.5 Background Neutron Discrimination

One of the objectives of the experiment was to measure the neutron energy spectrum produced by interactions in the upstream target and, in addition, to measure the energy spectrum of neutrons created, or scattered, by interactions in the downstream wall or elsewhere in the room. Events created in the liquid scintillator detectors by neutrons from the upstream target were separated from all other neutron events by periodically placing a neutron absorber directly between the detector and the center of the upstream target. The absorbers, referred to as “shadow bars”, were 12.7-cm diameter cylinders of iron that were either 1-m long or 2-m long. The 2-m shadow bar was used for the liquid scintillator detectors at 10°, 30°, and 45°, and the 1-m shadow bar was used at 60°, 80°, and 135°. Figure 5 shows the shadow bars aligned in front of the detectors at 45° and 135°, with the bars pointing towards the center of the 20 g/cm^2 polyethylene target. The 60 g/cm^2 polyethylene downstream target is at the end of the beam line.

Figure 5. The 2-m and 1-m long shadow bars (white steel cylinders) aligned between the center of the 20 g/cm^2 upstream polyethylene target and the 45° and 135° liquid scintillator detectors.

Data acquired with the shadow bar in front of the detector were used to determine the contributions from downstream target and room-scattered neutrons; data acquired with no shadow bar were used to determine the contribution from all sources (room-scattered, downstream target, and upstream target). By subtracting the shadow bar data from the non-shadow bar data, the contribution from the upstream target only can be determined.

For each beam species, energy, and upstream target material and thickness, there were four configurations (referred to as "runs") of shadow bar placement in front of the liquid scintillators (beam left). One configuration had no shadow bars in place, the second configuration had the shadows bars placed at 10° and 60°, the third at 30° and 80°, and the fourth at 45° and 135°.

II.6 Data Acquisition

A detected event was defined as the coincidence between an incident beam particle and a signal created in any of the "trigger" detectors. On beam left, the trigger detectors were the liquid scintillators, and on beam right, the trigger detectors were the solid plastic scintillators placed in front of the NaI detectors. An incident beam particle was defined as the coincidence between signals from the two "start" scintillators. Furthermore, the pulse heights from

coincident events in both start scintillators were used to select primary beam particles and eliminate any beam particles that were not of the desired beam species. Such particles can be present due to fragmentation in the beam exit window or air before striking the start scintillators, with a further contribution from ions having the same rigidity as the primary beam but with a different charge.

Beam particles were accelerated and delivered to the NSRL irradiation room by the Booster Synchrotron for the species and energies listed in Table 2. Beam particles were contained within bunches referred to as "spills" from the Booster every 4 – 6 seconds, with spill length varying between 0.3 and 3.5 seconds. The period and length of the spills depended on beam species and energy, with shorter spills generally associated with the highest energy beams. Beam currents were held to 1000 – 2000 particles per spill to limit pileup and keep experimental livetime reasonably high. The beam spots were small in diameter, varying between 0.5 and 1 cm (FWHM).

Data was acquired in list-mode (event-by-event) with an event processing time of 210 μs. The following information was recorded for each event:

- Energy deposited (PMT collected charge) in every scintillator
- PMT collected charge during the first 25 ns of the current pulse from the liquid scintillators
- Attenuated total and partial charge collected from events in the liquid scintillators
- Time-of-event in each trigger detector and start scintillator
- Clock signal synchronizing event with the spill
- Bit-mask indicating which detector(s) had a valid signal in the event

In addition to the event-by-event logging of data, cumulative scalers indicating the number of triggered events, number of processed events, and number of events in each detector were collected over the entire run.

All reported particle energies correspond to their energies at the point of detection and were determined either through the use of time-of-flight techniques, or in the case of downstream and background neutrons, by a pulse height deconvolution technique. The point of detection is determined by the trigger detectors, which in the case of neutrons and charged particles detected at beam left, are the liquid scintillators, and in the case of charged particles measured at beam right, are the plastic scintillators directly in front of the NaI detectors.

Interactions may occur at any depth in the upstream target. Variations in this dimension, along with variations in the kinematics of the reactions, result in a range of particle energies at the target exit, which are further reduced in a charge- and energy-dependent manner by traversing air before reaching a detector. Measured flight times are influenced by all of these variables, which must be carefully accounted for when comparing to model predictions of differential yields.

III Summary

Details of an accelerator-based experiment relevant to shielding in space have been given to allow for the accurate input to transport models used for benchmark comparisons between measured data and calculations. The experiments were conducted at the NSRL facility at Brookhaven National Laboratory between 2016 and 2017. Once published, the measured data will become publicly available through data archives at the University of Tennessee or by requests to the authors of this paper.

Acknowledgements

This work was supported by the National Aeronautics and Space Administration (United States) through Grants No. NNX15AD89A and NNX17AI10A. We gratefully acknowledge I-Hung Chiang and Rory Rosselot for their assistance at the NSRL facility, and John Norbury, Tony Slaba and Steve Blattnig for their helpful discussions on data needs.

IV References

[1] Tony C. Slaba, Amir A. Bahadori, Brandon D. Reddell, Robert C. Singleterry, Martha S. Clowdsley, Steve R. Blattnig, “Optimal shielding thickness for galactic cosmic ray environments”, Life Sci. Space Res. **12**, 1-15 (2017) DOI 10.1016/j.lssr.2016.12.003

[2] A. Ferrari, P.R. Sala, A. Fasso, J. Ranft, “FLUKA: A Multi-Particle Transport Code”, CERN 2005-10 / SLAC-R-773 (2005)

[3] S. Agostinelli et al., “GEANT4 – a simulation toolkit” Nucl. Instrum. Meth. A, 506, 250-303 (2003) DOI 10.1016/S0168-9002(03)01368-8

[4] J. T. Goorley, “MCNP6.1.1-Beta Release Notes” Los Alamos National Laboratory Technical Report LA-UR-24680 (2014)

[5] T. Sato, K. Niita, N. Matsuda, S. Hashimoto, Y. Iwamoto, S. Noda, T. Ogawa, H. Iwase, H. Nakashima, T. Fukahori, K. Okumura, T. Kai, S. Chiba, T. Furuta, L. Sihver, “Particle and heavy ion transport code system PHITS, version 2.52”, J. Nucl. Sci. Technol. **50**, pp. 913-923 (2013)

[6] J. W. Wilson, T. C. Slaba, F. F. Badavi, B. D. Reddell, A. A. Bahadori, “Advances in NASA radiation transport research: 3DHZETRN”, Life Sci. Space Res. **2**, 6-22 (2014)

[7] J. W. Norbury, J. Miller, A. M. Adamczyk, L. H. Heilbronn, L. W. Towsend, S. R Blattnig, R. B. Norman, S. B. Guetersloh, and C. J. Zeitlin, “Review of Nuclear Physics Experiments for Space Radiation”, *NASA TP 2011-217179* (2011).

[8] J. W. Norbury, J. Miller, A. M. Adamczyk, L. H. Heilbronn, L. W. Towsend, S. R Blattnig, R. B. Norman, S. B. Guetersloh, and C. J. Zeitlin, “Nuclear data for space radiation”, Radiat. Meas. **47**, 315-363 (2012). DOI 10.1016/j.radmeas.2012.03.004

[9] J. W. Wilson, M. Kim, W. Schimmerling, F. F. Badavi, S. A. Thibeault, F. A. Cucinotta, L. J. Shinn, R. Kiefer, “Issues in Space Radiation Protection: Galactic Cosmic Rays”, Health Phys. 68, 50-58, 1995

[10] S. Guetersloh, C. Zeitlin, L. Heilbronn, J. Miller, T. Komiyama, A. Fukumura, Y. Iwata, T. Murakami, and M. Bhattacharya, “Polyethylene as a radiation shielding standard in simulated cosmic-ray environments”, *Nucl. Instrum. Meth*. **B252**, 319-332 (2006). DOI 10.1016/j.nimb.2006.08.019

Tables

Table 1: The configurations of target materials and thicknesses used during the experiments conducted at the NSRL.

Upstream target material, thickness (g/cm^2)	Downstream target material, thickness (g/cm^2)
Al (20)	Al (60)
Al (40)	Al (60)
Al (60)	Al (60)
Polyethylene (20)	Polyethylene (60)
Polyethylene (40)	Polyethylene (60)
Polyethylene (60)	Polyethylene (60)
Al (10) + Polyethylene (10)	Polyethylene (60)
Al (10) + Polyethylene (50)	Polyethylene (60)

Table 2. Beam species and energies used for the NSRL thick target measurements. Reported energies are the energies incident upon the beam line exit window into the NSRL irradiation room. Uncertainties for beam energies, indicated in parentheses, are less than or on the order of 1%

Beam species	Beam energies (MeV/nucleon)
Protons	400(3), 800(6), 2500(15)
^{4}He	400(3), 800(6), 1500(10)
^{12}C	400(3), 800(6), 1400(10)[a], 1500(10)
^{28}Si	400(3), 800(6), 1470(10)[b], 1500(10)
^{56}Fe	400(3), 800(6), 1470(10)[b], 1463(10)[c]

[a] energy used for pure polyethylene and (Al+polyethylene) combination upstream targets

[b] energy used for pure Al upstream targets

[c] energy used for pure polyethylene targets

Table 3. EJ-301 and EJ-309 liquid scintillator information

Detector type	Light output (% anthracene)	Density (g/cm^3)	C atoms per cm^3	H atoms per cm^3	# photons per 1 MeV electron
EJ-301	78	0.874	$3.98x10^{22}$	$4.82x10^{22}$	12,000
EJ-309	80	0.959	$4.35x10^{22}$	$5.43x10^{22}$	12,300
EJ-204	68	1.023	$4.68x10^{22}$	$5.15x10^{22}$	10,400

Figures

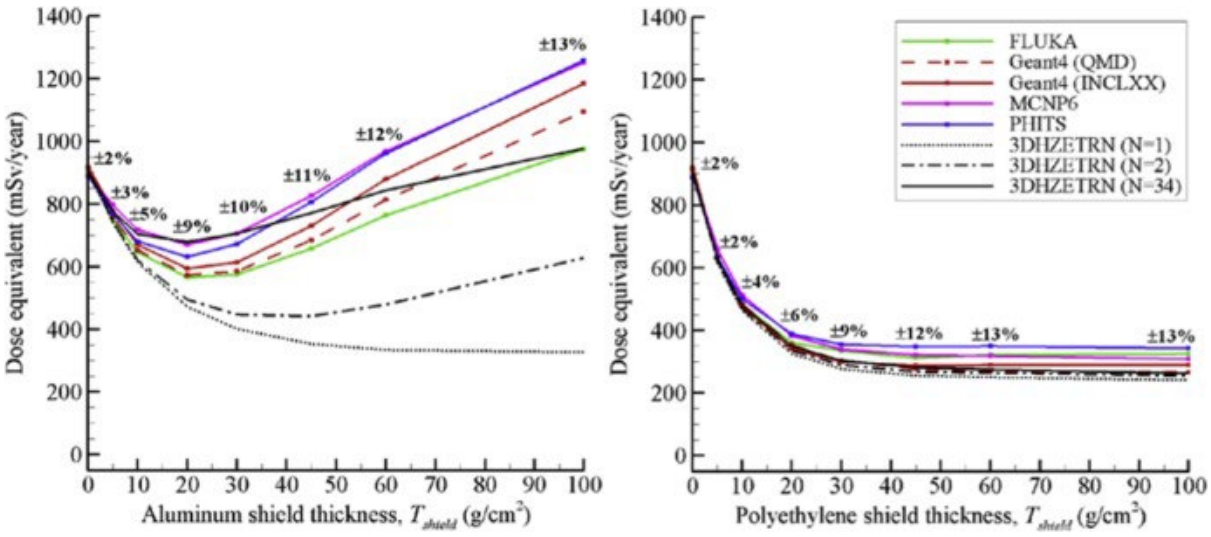

Figure 1. Dose equivalent from neutrons and ions as a function of aluminum (left) and polyethylene (right) shield thickness for the full GCR boundary condition.

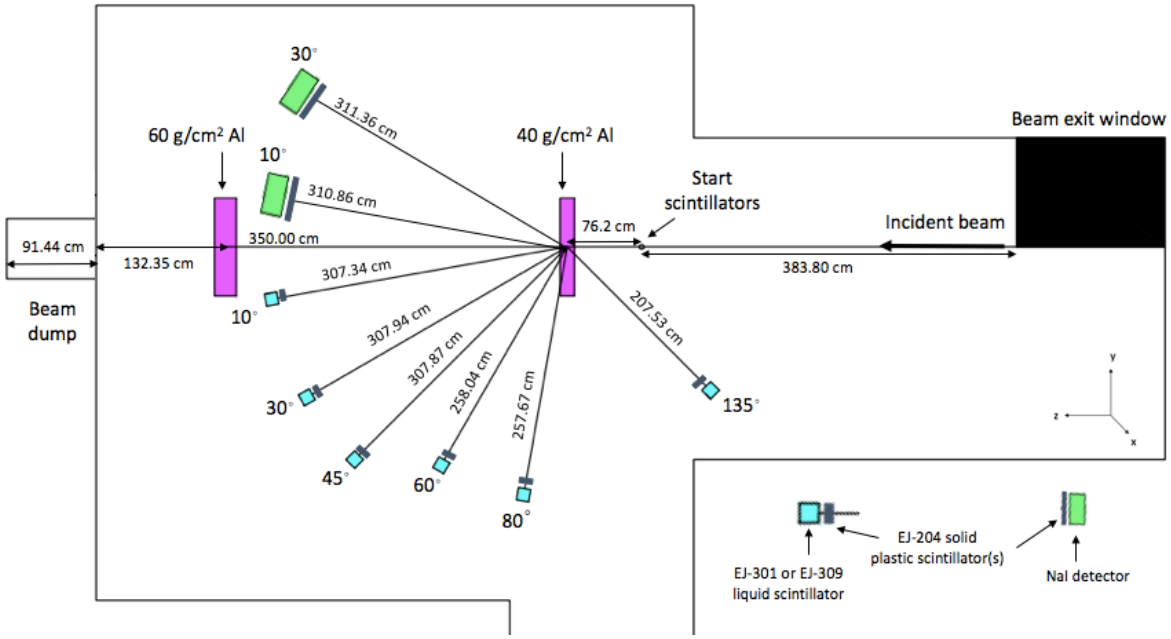

Figure 2. A schematic of the experimental setup in the NSRL irradiation room. Targets are shown in purple, liquid scintillators are shown in blue, and NaI detectors are shown in green. Solid plastic scintillators are shown in black. Not shown are the second solid plastic scintillators that were placed at the sides of the liquid scintillators

Figure 3. From left to right, the 80°, 60° and 45° liquid scintillator arrays with their accompanying solid plastic detectors. The liquid scintillators are the cylindrical detectors (aluminum housing), and the solid plastic scintillators are the black, 5-inch by 5-inch detectors

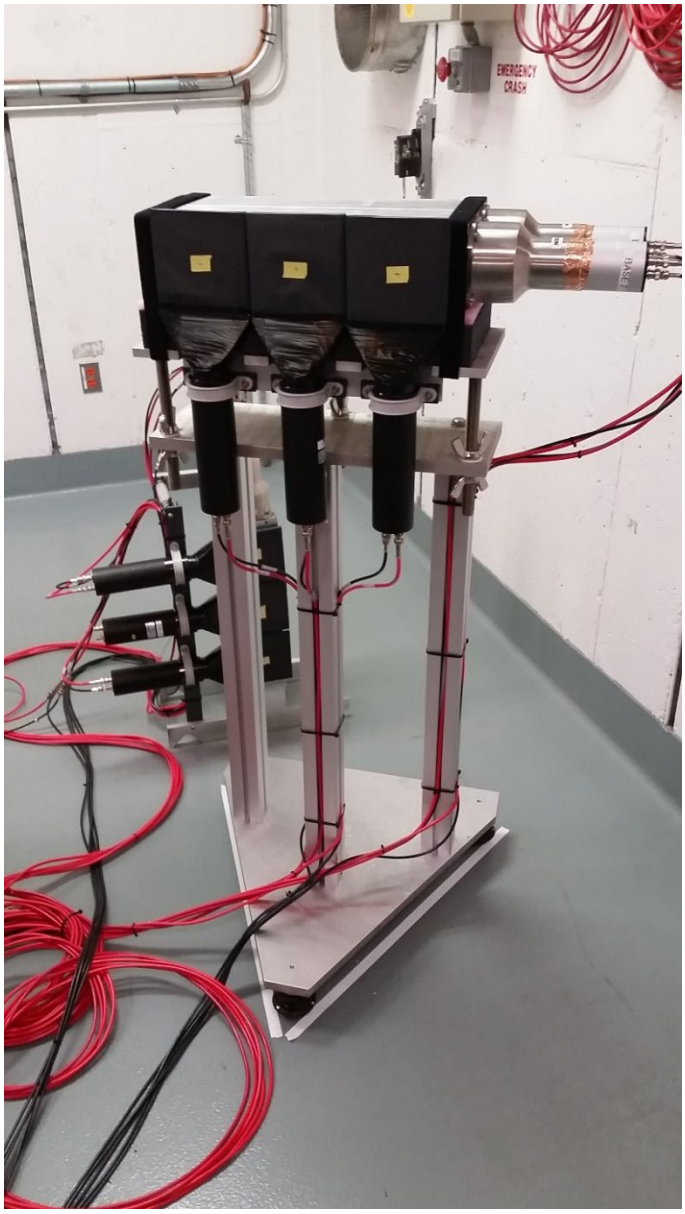

Figure 4. The 30° NaI detector array and stand. The three, square plastic scintillators are mounted directly in front of the two NaI detectors. The phototubes and bases for the NaI detectors can be seen at the right.

Figure 5. The 2-m and 1-m long shadow bars (white steel cylinders) aligned between the center of the 20 g/cm^2 upstream polyethylene target and the 45° and 135° liquid scintillator detectors.

1